Provided for non-commercial research and education use.
Not for reproduction, distribution or commercial use.

This article appeared in a journal published by Elsevier. The attached copy is furnished to the author for internal non-commercial research and education use, including for instruction at the authors institution and sharing with colleagues.

Other uses, including reproduction and distribution, or selling or licensing copies, or posting to personal, institutional or third party websites are prohibited.

In most cases authors are permitted to post their version of the article (e.g. in Word or Tex form) to their personal website or institutional repository. Authors requiring further information regarding Elsevier's archiving and manuscript policies are encouraged to visit:

http://www.elsevier.com/copyright

Author's personal copy

Solid State Communications 149 (2009) 408–411

Contents lists available at ScienceDirect

Solid State Communications

journal homepage: www.elsevier.com/locate/ssc

Monovacancy and substitutional defects in hexagonal silicon nanotubes

Gunn Kim [a,*], Suklyun Hong [b,*]

[a] BK21 Physics Research Division and Department of Physics, Sungkyunkwan University, Suwon 440-746, Republic of Korea

[b] Department of Physics and Institute of Fundamental Physics, Sejong University, Seoul 143-747, Republic of Korea

ARTICLE INFO

Article history:
Received 26 September 2008
Received in revised form
4 December 2008
Accepted 4 December 2008
by J.R. Chelikowsky
Available online 13 December 2008

PACS:
71.15 Mb
71.55.-i
73.20.At

Keywords:
A. Silicon nanotube
C. Monovacancy
C. Substitutional defects
D. Electronic structure

ABSTRACT

We present a first-principles study of the geometrical and electronic structures of a hexagonal single-walled silicon nanotube with a monovacancy or a substitutional defect. The B, C, N, Al and P atoms are chosen as substitutional impurities. It is found that the defect such as a monovacancy or a substitutional impurity results in deformation of the hexagonal single-walled silicon nanotube. In both cases, a relatively localized unoccupied state near the Fermi level occurs due to this local deformation. The differences in geometrical and electronic properties of different substitutional impurities are discussed.

© 2008 Elsevier Ltd. All rights reserved.

1. Introduction

Cubic-diamond bulk silicon is a very well-known semiconducting material with an energy band gap of 1.2 eV. Unlike the cubic-diamond silicon, it would be difficult to form one-dimensional single-walled silicon nanotubes (SiNTs) mainly because silicon prefers sp^3 to sp^2 hybridization. Bai and his co-workers [1] suggested, however, that SiNTs could be formed by the top-to-top stacking of square, pentagonal and hexagonal silicon structures and showed using *ab initio* calculations that the pentagonal and hexagonal SiNTs may be locally stable in vacuum and be metallic. Their work provided computational evidence for a possible existence of such one-dimensional silicon nanostructures, although those structures have not been observed experimentally yet.

At this point, it would be valuable to theoretically investigate the interaction of adsorbates with these silicon nanostructures as well as stability and related electronic structure of defective SiNTs. In fact, Si nanostructures may be passivated or oxidized under ambient conditions. As reported in Ref. [1], in our model of the Si nanostructure (the hexagonal single-walled SiNT), each Si atom has a coordination number of four. It should be compared with a different type of the SiNTs [2] having a hexagonal network like the carbon nanotube (CNT), where each Si atom has a coordination number of three. Very recently, we studied the hydrogen adsorption on hexagonal single-walled SiNTs to consider the possibility of SiNTs as a hydrogen storage material [3]. It was found that hydrogen molecules are physisorbed with binding energy less than 0.1 eV. In this Communication, from the viewpoint of stability for SiNTs, we investigate the modification in the geometrical and electronic structures of hexagonal SiNTs with a monovacancy or a substitutional defect.

2. Calculational methods

First-principles pseudopotential calculations are carried out based on the density functional theory [4,5] within the generalized gradient approximation for the exchange–correlation functional. The potential is described with the Vanderbilt-type ultrasoft pseudopotential [6]. Wave functions are expanded in a plane wave basis set with an energy cutoff of 21 Ry implemented in the Quantum Espresso code [7]. As a model system, we choose a hexagonal SiNT with a monovacancy or a substitutional defect. B, C, N, Al and P atoms are chosen as substitutional impurities. All chosen model systems are treated by a supercell with the periodic boundary condition. The supercell in the lateral direction is as large as 19.2 Å, which is 16 times the minimal unit cell

* Corresponding author. Tel.: +82 31 299 6508; fax: +82 31 290 5954.
E-mail addresses: kimgunn@skku.edu, kimgunn@gmail.com (G. Kim), hong@sejong.ac.kr (S. Hong).

0038-1098/$ – see front matter © 2008 Elsevier Ltd. All rights reserved.
doi:10.1016/j.ssc.2008.12.010

Author's personal copy

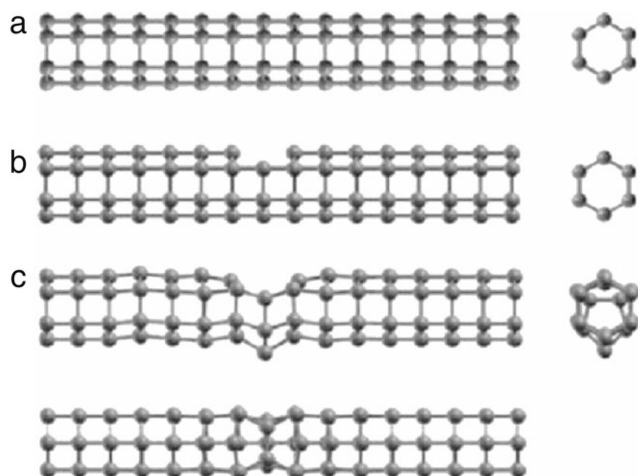

Fig. 1. Schematic ball-and-stick models of (a) a pristine hexagonal SiNT, (b) an SiNT with a monovacancy before relaxation, and (c) an SiNT with a monovacancy after relaxation, respectively.

(16 × 2.4 Å) in the tube axis direction. The structures are relaxed until the Hellmann–Feynman forces are smaller than 0.05 eV/Å. The Brillouin-zone integration is done within the Monkhorst-Pack scheme [8], using 1 × 1 × 4 *k*-point sampling.

To understand the features of charge distribution of our models, we perform the Mulliken population analysis using a numerical atomic orbital basis set in the OpenMX code [9,10] with a kinetic energy cutoff of 150 Ry. For this Mulliken population analysis, norm-conserving Kleinman–Bylander pseudopotentials [11,12] are employed.

3. Results and discussion

First, we calculate hexagonal SiNTs with or without a monovacancy shown in Fig. 1. If a single Si atom is removed from the nanotube, two of four Si atoms around the vacancy rebond (bond length of 2.42 Å) to form a pentagonal cross section. In the case of cubic-diamond bulk silicon, the lattice constant is 5.43 Å, which corresponds to the Si–Si bond length of 2.35 Å. It is noted that a buckled honeycomb planar structure [2] of silicon has the average Si–Si bond length of 2.2 Å. The rebonded two atoms are perpendicular to the tube axis. Although other two Si atoms have dangling bonds even after the relaxation, their dangling bond characters become weak since the two Si atoms make strong bonds with three adjacent Si atoms (bond lengths of 2.32–2.36 Å). The formation energy ($=E_{perfect} - E_{vacant} - E_{Si}$) of a single vacancy in an SiNT is 16.3 eV (4.07 eV per bond). In the optimized structure, the Si atom on the opposite side to the monovacancy is protruded by ∼1 Å from the surface of the nanotube. The bonding angle with respect to this protruded Si atom at the pentagonal defect is 89.6° as shown in Fig. 1(c). Molecular dynamics (MD) simulations revealed that pentagonal and hexagonal SiNTs can remain stable [1,2]. Our MD simulation result shows that the SiNT with a monovacancy is somewhat distorted but not broken at 600 K.

Such locally large distortion even at 0 K may affect the band structure and charge distribution of the SiNT. In terms of the

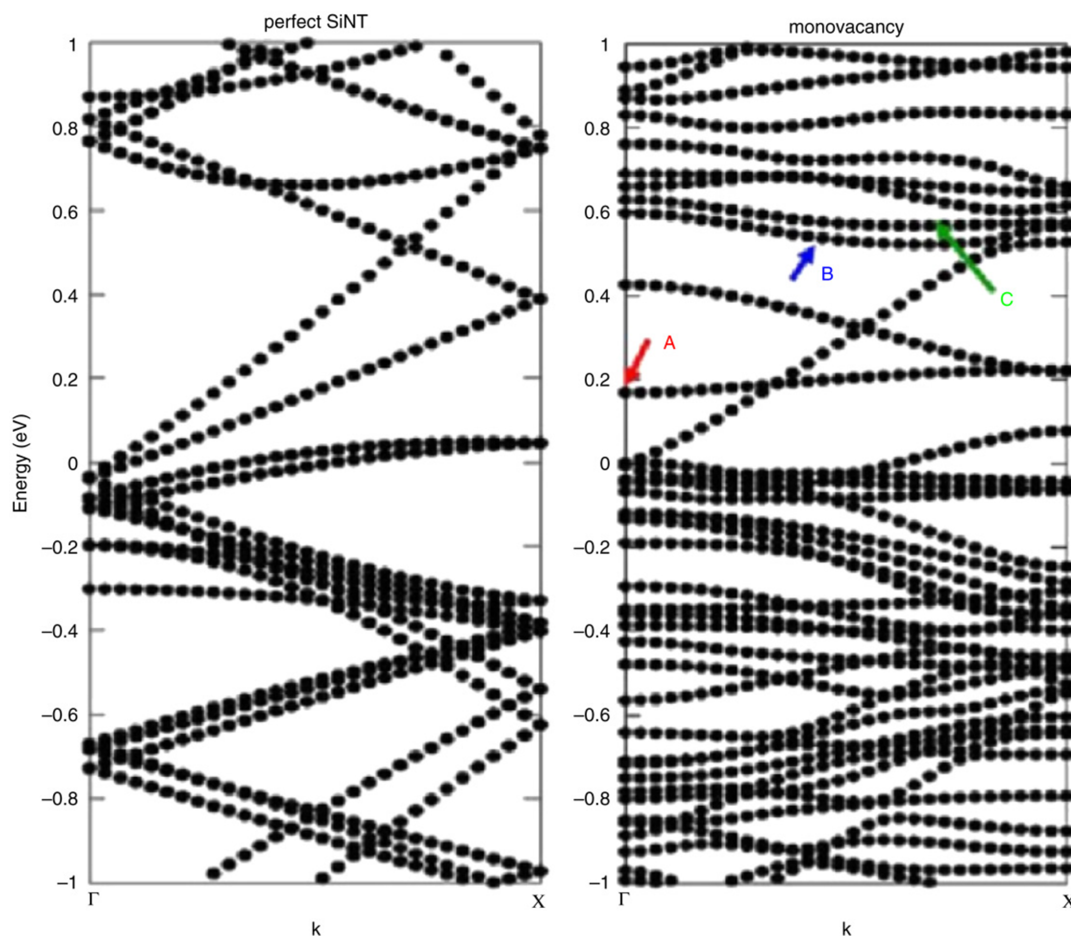

Fig. 2. Band structures for the SiNT structures corresponding to a pristine SiNT (left) and an SiNT with a monovacancy after relaxation (right). States A, B, and C are ULSs. The Fermi level is set to zero. Localized states occur originating from a monovacancy.

Author's personal copy

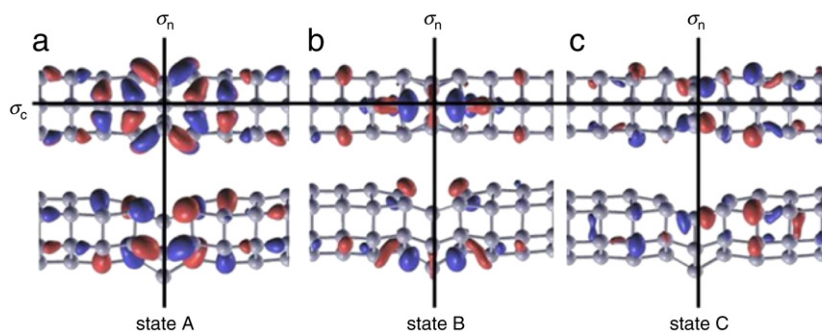

Fig. 3. Isodensity surface plots of the ULSs at Γ that come from the distortion due to the presence of a monovacancy: Top and side views for a ULS (state A) near +0.2 eV due to the local deformation are shown in (a), and those for two ULSs (states B and C) near +0.6 eV due to the pentagonal defect are in (b) and (c). The values for the red and blue isodensity surfaces are $\pm 0.02\ e/a_0^3$, where the sign is that of the wave function and $a_0 = 0.529$ Å, the Bohr radius. (For interpretation of the references to colour in this figure legend, the reader is referred to the web version of this article.)

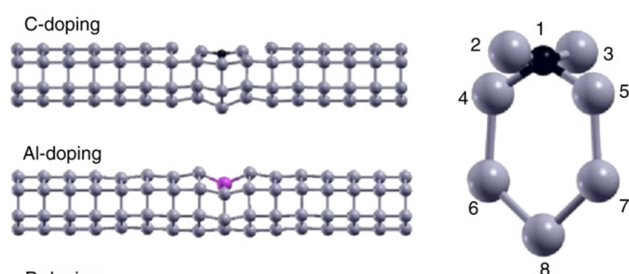

Fig. 4. Schematic ball-and-stick models of relaxed hexagonal SiNTs with substitutional impurities. The grey, black, pink, and yellow balls represent a silicon, carbon, aluminum, and phosphorus atoms, respectively. (For interpretation of the references to colour in this figure legend, the reader is referred to the web version of this article.)

Mulliken population analysis, we find an interesting feature. The protruded Si atom on the opposite side to the vacancy obtains 0.12 e and its adjacent Si atoms lose electrons: Each of two adjacent Si atoms in the tube axis direction loses 0.025 e, while each of two in the circumference direction loses 0.035 e. On the other hand, the two rebonded Si atoms lose 0.073 e, respectively.

As mentioned above, the left band plot of Fig. 2 clearly shows that the hexagonal SiNT has the metallic character [1]. When a monovacancy is formed in the SiNT, the energy band structure is changed accordingly. There are prominent localized states above the Fermi level. In particular, a localized state (state A) originating from the structure distortion gives a flat band around 0.2 eV above the Fermi level as denoted by a downward arrow in the right band plot of Fig. 2. The isodensity surface plot of this unoccupied localized state (ULS) is presented in Fig. 3(a). In addition, a pentagon as a topological defect also gives rise to two ULSs (states B and C) near +0.6 eV as depicted by upward arrows in the right band plot of Fig. 2. Interestingly, Figs. 3(b) and (c) show that the localized states by a pentagonal defect are split into even and odd parity states with respect to the mirror planes (σ_c and σ_n) containing and normal to the nanotube axis, respectively.

Next, we present the geometrical and electronic structure of hexagonal SiNTs with substitutional impurity. Fig. 4 shows the relaxed geometries of SiNTs for carbon, aluminum or phosphorus atom substitutions. For the case of the C doping, the C–Si bond lengths (C1–Si2 and C1–Si3), d_{12} and d_{13}, parallel to the tube axis are 1.93 Å and those (C1–Si4 and C1–Si5), d_{14} and d_{15}, perpendicular to the axis are 1.92 Å. These bond lengths and angles (see below) in the SiNT with C doping are listed in Table 1, along with the cases of B, N, Al and P doping. Here, the numbers

Table 1
Calculated bond lengths and angles in SiNTs with substitutional impurities.

Impurity	B	C	N	Al	P
d_{12}, d_{13} (Å)	2.00	1.93	2.05	2.58	2.50
d_{14}, d_{15} (Å)	2.03	1.92	1.85	2.61	2.30
$\angle 213$ (°)	177.4	165.8	162.3	133.1	145.5
$\angle 415$ (°)	115.0	120.6	119.3	140.3	102.3

(i, j, k) in d_{ij} and $\angle ijk$ represent the atoms labeled likewise in Fig. 4. The C atom is buckled inward by ~0.4 Å and the Si8 atom on the opposite side to the C dopant is protruded outward by ~0.6 Å. Owing to the strain effect, Si–Si bond breaking occurs near the defect site. The bond angle between C and adjacent Si atoms, ∠Si2C1Si3 (∠213), parallel to the tube axis are 165.8° and ∠Si4C1Si5 (∠415) perpendicular to the axis is 120.6°. In the case of B and N substitutional defects, the trends of bond lengths and bonding angles are similar to those of the C impurity (see Table 1). For B, C, and N impurities having the atomic radii smaller than that of Si, all of them are buckled inward.

For the Al doping, the Al–Si bond lengths parallel and perpendicular to the tube axis are 2.58 and 2.61 Å, respectively. Here the Al atom is buckled inward by ~0.7 Å and the Si atom on the opposite side to the Al dopant is buckled inward by ~0.1 Å. The bond angle between Al and adjacent Si atoms parallel to the tube axis are 133.1° and that perpendicular to the axis is 140.3°. In contrast, the P dopant shows an outward buckling by ~0.3 Å. Such a trend is shown for boron nitride nanotubes [13], where nitrogen atoms are buckled outward and boron atoms are inward, which is associated with unpaired electrons. For the P doping, the Si atom on the opposite side to the P dopant is buckled outward by ~0.3 Å. The P–Si bond lengths parallel and perpendicular to the tube axis are 2.50 and 2.30 Å, respectively. The bond angle between P and adjacent Si atoms parallel to the tube axis is 145.5° and that perpendicular to the axis is 102.3°.

When substituted, the C atom donates 0.25 e to the SiNT and the protruded Si atom on the opposite side to the C atom obtains 0.09 e. Similarly, the boron (nitrogen) impurity also donates 0.23 e (0.03 e) to the SiNT and the protruded Si atom on the opposite side to the boron (nitrogen) atom obtains 0.07 e (0.11 e). In contrast, the P atom obtains 0.23 e from the SiNT and the protruded Si atom on the opposite side to the P atom obtains 0.014 e. In the case of the Al impurity, there is no practical electron transfer between the SiNT and the Al atom (0.003 e). It is thus found that the large displacement of the Si atom opposite to a substitutional impurity is associated with the large electron transfer.

Fig. 5 shows band structures for the substitution of B, C, N, Al and P atom. The relatively flat bands of ULSs around 0.1–0.2 eV above the Fermi level are denoted by red arrows. We find that these ULSs originate mainly from the structure distortion. Their origin

Author's personal copy

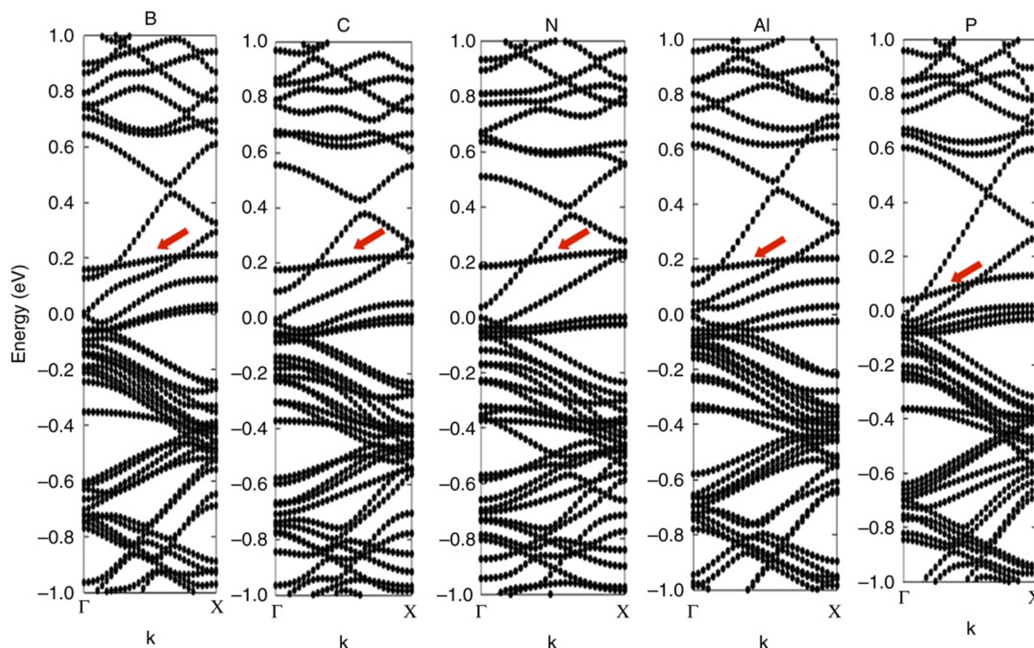

Fig. 5. Band structures for boron, carbon, nitrogen, aluminum and phosphorus atom substitutions. Arrows indicate the ULSs originating from the deformation near the Fermi level.

is the same as that of the flat band (denoted by a downward red arrow in Fig. 2(c)) of ULS produced by the presence of vacancy. Especially, since the geometrical structure of SiNT with C-doping in Fig. 4 is almost the same as that of SiNT with a monovacancy in Fig. 1(c) except the substituted carbon atom itself, the isodensity surface plot of the ULS in C-doped SiNT is expected to be almost the same as that shown in Fig. 3. Moreover, each impurity (B, C, N, Al or P) atom results in more or less flat bands, i.e., localized states (not shown here), about 2.0 eV below or above the Fermi level. In contrast to the other impurities in our models, the Al impurity state has relatively high density of states of Al near the ULS indicated by the arrow in Fig. 5 and is well hybridized with the ULS. On the other hand, as shown in Figs. 2 and 5, the occupied states right below the Fermi level have less dispersive bands. However, their electron densities are not localized near substitutional defect sites but somewhat delocalized at other regions of the SiNT.

4. Conclusion

In summary, structural and electronic property changes caused by various vacancy or substitutional defects are studied in the hexagonal SiNTs using *ab initio* pseudopotential calculations. The C, Al and P atoms are chosen as substitutional impurities. It is found that a defect such as a monovacancy or a substitutional impurity results in deformation of the nanotube. The relatively localized states near the Fermi level shown in both cases with a monovacancy or an impurity occur due to this local deformation. When we consider the realistic situation of the randomly distributed defects, there would be somewhat broadened density of states originating from almost degenerate localized states.

Acknowledgements

G.K. was supported by the post BK21 project of Ministry of Education, Science and Technology (MEST). S.H. was supported by the KOSEF grant funded by MEST (Center for Nanotubes and Nanosructured Composites R11-2001-091-00000-0).

References

[1] J. Bai, X.C. Zeng, H. Tanaka, J.Y. Zeng, Proc. Natl. Acad. Sci. 101 (2004) 2664.
[2] E. Durgun, S. Tongay, S. Ciraci, Phys. Rev. B 72 (2005) 75420.
[3] J. Ryou, S. Hong, G. Kim, Solid State Commun. 148 (2008) 469.
[4] P. Hohenberg, W. Kohn, Phys. Rev. B 136 (1964) 864.
[5] W. Kohn, L.J. Sham, Phys. Rev. 140 (1965) A1133.
[6] D. Vanderbilt, Phys. Rev. B 41 (1990) R7892.
[7] S. Baroni, A. Dal Corso, S. de Gironcoli, P. Giannozzi, Available on: http://www.pwscf.org.
[8] H.J. Monkhorst, J.D. Pack, Phys. Rev. B 13 (1976) 5188.
[9] T. Ozaki, Phys. Rev. B 67 (2003) 55108.
[10] T. Ozaki, H. Kino, Phys. Rev. B 69 (2004) 195113.
[11] N. Troullier, J.L. Martins, Phys. Rev. B 43 (1991) 1993.
[12] L. Kleinman, D.M. Bylander, Phys. Rev. Lett. 48 (1982) 1425.
[13] A. Rubio, J.L. Corkill, M.L. Cohen, Phys. Rev. B 49 (1994) 5081.